Atomic Spectroscopy

Article

Magnesium Isotopic Analysis of Biochemical Reference Materials Using MC-ICP-MS: A Dataset for Dietary and Human Tissue

Di Wang,[a,b] Guilin Han, [a,b,*] Qian Zhang,[c] and Wenqian Sun [a,b]

[a] State Key Laboratory of Geomicrobiology and Environmental Changes, Institute of Earth Sciences, China University of Geosciences (Beijing), Beijing 100083, P. R. China

[b] Frontiers Science Center for Deep-time Digital Earth, China University of Geosciences (Beijing), Beijing 100083, P. R. China

[c] Institute of Geographic Sciences and Natural Resources Research, Chinese Academy of Sciences, Beijing 100101, P. R. China

Received: *November 09, 2025;* ***Revised:*** *November 30, 2025;* ***Accepted:*** *December 03, 2025;* ***Available online:*** *December 03, 2025.*

DOI: 10.46770/AS.2025.112

ABSTRACT: Magnesium (Mg) isotopic compositions help decode the complex biogeochemical cycling of Mg in surficial environments. Accurate measurement of Mg isotopes in biological samples requires reference materials with established isotopic compositions, which ensure analytical quality and allow interlaboratory comparison. By employing Nu Plasma III multi-collector inductively coupled plasma-mass spectrometry (MC-ICP-MS), this study establishes a high-precision Mg isotopic dataset for sixteen biological reference materials. The measured δ^{26}Mg values of extra nine reference materials (plant leaves, rocks, and seawater) consistently agree well with references values, confirming the reliability of analytical methodology used in this study. The results reveal the variations for δ^{26}Mg values exceeding 2.2‰ across the food web. Plant leaves are characterized by low δ^{26}Mg values (–0.52‰ ± 0.04‰ ~ –1.28‰ ± 0.03‰), whereas cereals and animal organs exhibit heavier values (up to 0.97‰ ± 0.05‰ for pork liver). The δ^{26}Mg values of scallops (GSB-15), spirulina (GSB-16), and prawn (GSB-28) cluster together with lighter values, representing a marine-derived isotopic end-member for coastal populations. Human hairs (–0.88‰ ± 0.04‰) present an integrated isotopic signature intermediate between major dietary end-members. This dataset expands the Mg isotopic compositions of major dietary and human tissue reference materials, supporting the essential laboratory comparison of isotope analyses and facilitating researches into the Mg biogeochemical cycle.

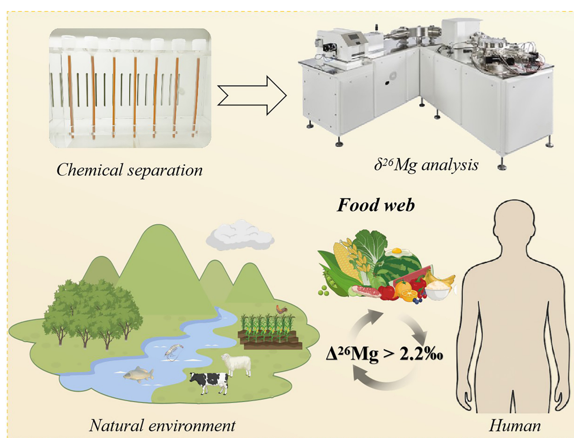

INTRODUCTION

Magnesium (Mg) is an essential macronutrient that plays a critical role in biogeochemical cycling and human health. It is widely distributed in the surface environment and enters biological systems through multiple pathways, coordinating vital physiological processes such as photosynthesis,[1] cellular energy metabolism,[2] enzyme activation,[3] and nucleic acid stability.[4] In humans, Mg regulates numerous biochemical functions (*e.g.*, adenosine triphosphate utilization, deoxyribonucleic acid repair, muscle contraction, and neurological regulation).[5,6] Growing evidence indicates that Mg homeostasis is associated with various disease.[7-9] Therefore, accurately tracking the biogeochemical processes of Mg from the environment into the human body is crucial for revealing its metabolic pathways and potential pathogenic mechanisms within biological systems.

Stable isotopes have emerged as important tracers for investigating element cycling on Earth's critical zone.[10,11] The three stable isotopes of Mg (^{24}Mg, ^{25}Mg, and ^{26}Mg) exhibit significant fractionation in natural environments and biological actions, with δ^{26}Mg values varying by more than 5‰ across different reservoirs.[12-14] This characteristic makes the Mg isotopic system a well tracer for studying Mg biogeochemical cycles [14,15] and biological metabolic processes.[16-18] More importantly, the Mg isotopic composition in human/animal tissues shows potential as a biomarker for evaluating Mg status and its implications for health and disease. This potential is realized through a combination of dietary source imprinting and internal metabolic fractionation.[19, 20] Preferential absorption of specific isotopes during metabolic processes (*e.g.*, enzymatic binding, renal handling) create a tissue-specific isotopic pool.[21, 22] Consequently, disruptions in Mg homeostasis caused by diseases can alter these fractionation patterns, making tissue δ^{26}Mg a sensitive indicator of metabolic status.[7, 23, 24] However, its application in health research is based on the principle of isotopic signal passed through the food chain. As dietary intake represents the primary route of Mg absorption in humans,[25] understanding the isotopic signatures of dietary Mg is important. Currently, although Mg isotope studies related to human diet remain limit, evidence from plants and animal models has revealed potential patterns of isotopic fractionation.[21, 23, 26] In plants, isotopic fractionation occurred with Mg transport during both root absorption and vascular mobility.[27, 28] This process occurs via both passive transport through the cation channels of the plasma membrane and active mechanisms facilitated by specific transport proteins.[29] This physiological fractionation creates distinct isotopic patterns across food sources. For example, leafy vegetables usually exhibit lower δ^{26}Mg values compared with cereal grains (*e.g.*, wheat).[30-32] These isotopic signals derived from plants are subsequently altered during further trophic level transferring. Martin et al.[26] found that herbivore teeth show lighter Mg isotopes compared to omnivores, with muscle tissues becoming enriched in ^{26}Mg along food chains. Animal tissues also display significant internal variations of Mg isotopic composition. Goff *et al.*[33] reported distinct δ^{26}Mg values between whole milk (–0.74‰) and bovine liver (0.52‰), while marine products show Mg isotopic compositions closer to the seawater signature. Although the relationship between human and diet remains poorly understood, a recent study revealed that the Mg isotopic characteristic of human tooth reflects staple food consumption patterns.[19] The results observed across different trophic levels position Mg isotopic system as a reliable tracer for investigating human dietary patterns and metabolic processes.

High-precision analysis of Mg isotopes has been made possible by techniques such as multi-collector inductively coupled plasma mass spectrometry (MC-ICP-MS) and standard-sample bracketing,[30,34] which effectively mitigate analytical biases. However, unlike geochemical studies supported by certified rock standards,[35-37] high-precision Mg isotopic data for biological reference materials remains limited, especially for dietary standards. Meanwhile, the quality control of biological matrix analysis continues to be constrained by the shortage of well-characterized biological reference materials. This lack of reliable benchmark values further impedes method validation and interlaboratory comparison. To provide essential baseline data to support the growing application of Mg isotopes in environmental and health research, this study presents high-precision Mg isotopic data for twenty-five reference materials, including rocks, solution, biological tissues and dietary products. Among them, the Mg isotopic compositions of sixteen biological reference materials were reported for the first time to ensure a foundation of reliable and comparable measurements.

EXPERIMENTAL

Chemical reagents and reference materials. The reagents involved in this study include three highly concentrated chemical reagents (BVIII grade, HNO_3, HCl, HF). Before used, they were purified by sub-boiling distillation using a Savillex DST-4000 system to minimize procedural blanks. A Cascada™ water purification system (Pall, USA) was used to filtrate ultrapure water (resistivity: 18.2 MΩ·cm). Prior to use, labware including tips, tubes, columns, and Savillex perfluoroalkoxy (PFA) beakers were subjected to systematic cleaning steps. Tubes and tips were sequentially heated on a hotplate at 90 °C for over 12 hours in 20% (v/v) HNO_3, 10% (v/v) HCl, and ultrapure water. Between each acid step, these items were rinsed three times with ultrapure water. Additionally, the PFA beakers and columns were cleaned with HNO_3 (1:1 v/v, prepared by diluting concentrated HNO_3 with ultrapure water) and HCl (HNO_3 : ultrapure water = 1:3 v/v), respectivily. Each step lasts over 12 hours at 90 °C, and all labware were thoroughly rinsed with ultrapure water between each acid step and upon completion. After the final cleaning step, all labware were evaporated to dryness. The AG 50W-X12 (200 ~ 400 mesh) cation exchange resin and standard micro-column (180 mm length, 4 mm ID, 2.3 mL bed volume) were utilized for chromatographic separation.

Table 1 shows the reference materials used in this study, including rocks (SDC-1 and BHVO-2), plants (GSB-1, GSB-5, GSB-6, GSB-11, GSB-14, GSB-17, GSB-18, GSB-19, GSV-1, GSV-3, GSV-4), animals (GSB-9, GSB-15, GSB-16, GSB-28, GSB-29), grain processing products (GSB-8, GBW10055, BW2025-5050 and BW2025-5051), human hair (GBW090101) and standard solutions (IAPSO seawater, Alfa-Mg). These reference materials were purchased from the United States Geological Survey, the Beijing WeiBiao Standard Science and Technology Ltd, the Academy of National Food and Strategic Reserves Administration, the Institute of Geophysical and Geochemical Exploration and the National Institute of Metrology, China.

Sample pretreatment and Mg purification. All experiments were carried out in a class-1000 clean laboratory setting at the Nu Surficial Environment and Hydrological Geochemistry

Table 1. The information of reference materials analyzed in this study

Type	Sample	Mg%	Description
Cereals	GSB-1	0.01	Rice
	Element-ZK-004	0.01	Rice Flour
	BW2025-5051	0.01	Rice Flour
Plant Leaves	GSB-5	0.15	Cabbage
	GSB-6	0.13	Spinach
	GSB-11	0.17	Citrus Leaves
	GSV-1	0.25	Bush Branches and Leaves
	GSV-3	0.52	Bush leaves
	GSV-4	0.06	Tea Leaves
Protein Sources	GSB-8	0.07	Milk Powder
	GSB-9	0.12	Chicken Meat
	GSB-29	0.05	Pork Liver
	GSB-15	0.07	Scallop
	GSB-28	0.12	Prawn
	GBW10055	0.19	Full-fat Soybean Flour
	BW2025-5050	0.11	Infant Formula Powder
Algae & Functional Foods	GSB-14	0.29	Laver
	GSB-16	0.21	Spirulina
	GSB-18	0.10	Ginseng
	GSB-19	0.19	Milkvetch Root
Human Tissue	HHS-1	0.04	Human Hair
	GBW09101	0.02	Human Hair
Geological End-member	BHVO-2	4.36	Basalt from Kilauea Hawaii, Halemaumau crater
	BCR-2	2.16	Basalt from Columbia River
Solution	Seawater	0.13	Seawater from the Atlantic Ocean (IAPSO)
	Alfa-Mg	1 mg/L	Solution state from Johnson Matthey company

Table 2. Instrumental parameters and collector configuration

Parameter	Description
Resolution mode	low
RF Power	1300 W
Nebuliser gas	30 Psi
Auxiliary gas	0.9 L/min
Cooling gas	13.0 L/l min
Cycles/Blocks	20/2
Integration time	10 s
Nebulizer	100 μl /min PFA nebuliser
Cones	standard 'wet' cone set
^{24}Mg background noise	< 1.5 mV
Collector configuration	L5(^{24}Mg), Ax(^{25}Mg), H6(^{26}Mg)

Laboratory (Nu-SEHGL), China University of Geosciences (Beijing), with sample processing under a class-100 laminar flow hood. An optimized digestion protocol for biological samples was implemented, modified from established methodologies [38, 39] to ensure efficient decomposition and high recovery rates. Sample digestion was carried out with a microwave digestion system (Multiwave PRO, Anton Paar, AT). Specifically, about 50 mg of each powdered sample was accurately weighed into 50 mL digestion vessels. Each vessel was added a mixed concentrated acid, including 6 mL HNO_3, 3 mL HCl, and 2 mL HF. To enhance the complete oxidation of organic components, samples were subjected to pre-digestion at ambient temperature for 12 h. Subsequently, microwave-assisted digestion was performed using a stepped heating program, which the temperature was gradually increased to 180°C and maintaining for 40 minutes. This heating cycle was duplicated to ensure complete digestion. The resulting solution was evaporated to dryness after cooling. Then the residual solid was treated twice with concentrated HNO_3 to achieve complete dissolution and homogenization of the sample.

Mg purification was conducted using ion-exchange chromatography with BioRad AG 50W-X12 resin, following the method established by Liu *et al.*[39] Prior to separation, the resin was pre-treated with two 3 mL aliquots of an acid mixture (1.5 mol/L HNO_3 + 0.1 mol/L HF). Then, sample solution containing approximately 10 μg of Mg was loaded into the prepared columns. Matrix elements were removed by elution with 17 mL of same acid mixture, followed by the collection of the Mg using 7 mL of the same eluent. The collected Mg solution was evaporated to dryness and subsequently drying down with concentrated HNO_3, finally redissolved in 2% HNO_3 for isotopic analysis. Elemental analysis confirmed effective separation of the matrix components, with a total recovery rate of Mg achieved at 99.7% ± 0.8%, indicating that the method could quantitatively recover Mg and completely separate it from the main matrix elements.

Mass spectrometry. The measurements of Mg isotopes were analyzed using a Nu Plasma III MC-ICP-MS (Nu Instruments, UK) at the Nu-SEHGL laboratory, and operating parameters are shown in Table 2. Sample introduction was automated with an ASX-110FR autosampler (Cetac Technologies, USA). The instrument configuration employed a standard wet cone assembly and a 0.1 mL/min PFA nebulizer operating under wet plasma conditions.

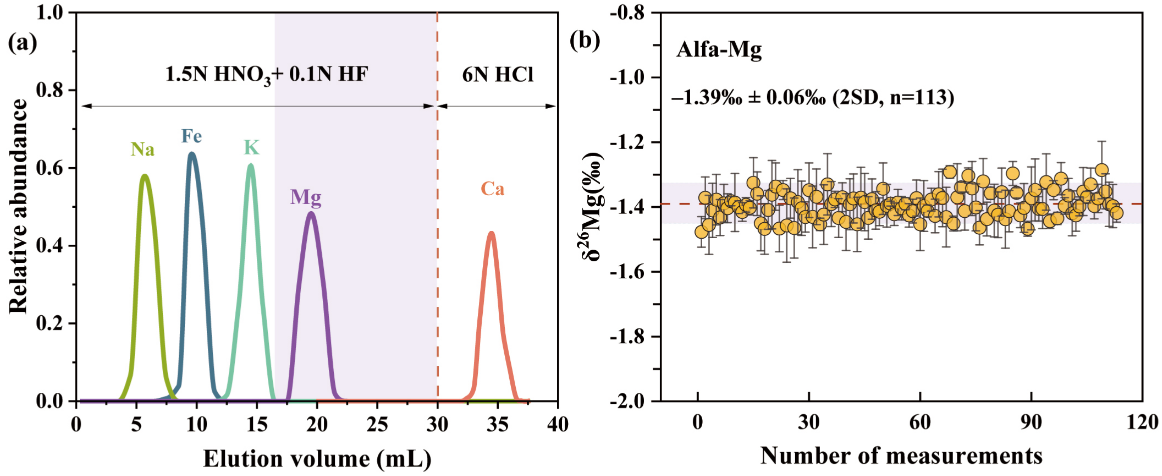

Fig. 1 (a) Elution curves for Mg separation (GSB-8); (b) Long-term analytical precision of Alfa-Mg (red dashed line represent the mean of $\delta^{26}Mg_{Alfa\text{-}Mg}$).

In this study, Faraday cups L5, Ax, and H6 were simultaneously used to collected ^{24}Mg, ^{25}Mg, and ^{26}Mg, respectively. Prior to analysis, the Faraday pre-amplifier bin was evacuated to establish an optimal static vacuum condition. Daily calibration procedures included Faraday gain calibration and background noise measurements. Through systematic optimization of ion source parameters, a stable signal intensity of approximately 15 V for ^{24}Mg was achieved using a 1 μg/mL Mg solution in low-resolution mode, and the ^{24}Mg signal in the nitric acid blank was less than 1.5 mV before the introduction of sample solutions and contributed less than 0.1% to the sample signals. The measurement protocol consisted of 2 blocks with 20 cycles per block, employing a magnet settling time of 2 s and an integration time of 10 s per measurement.

All analytical solutions were prepared in 2% (v/v) HNO_3. To minimize cross-contamination between samples, an extensive wash protocol was implemented comprising two sequential steps: 100 s with 5% HNO_3 followed by at least 100 seconds with 2% HNO_3. The 2% HNO_3 wash continued until the ^{24}Mg signal decreased below 1.5 mV, ensuring effective removal of residual Mg. Mass bias was corrected using the standard-sample bracketing (SSB) method. The $\delta^{26}Mg$ value represents the per mil deviation of sample isotopic composition from the reference standard, defined in equation (1):

$$\delta^{x}\mathrm{Mg}\ (‰)=\left[\frac{(^{x}\mathrm{Mg}/^{24}\mathrm{Mg})_{\mathrm{sample}}}{(^{x}\mathrm{Mg}/^{24}\mathrm{Mg})_{\mathrm{standard}}}-1\right]\times 1000 \qquad (1)$$

where x represents either mass number 25 or 26. Standard indicates the delta-zero reference material (Alfa-Mg) employed in the analysis, and $(^{x}Mg/^{24}Mg)$ standard was the mean of the reference results before and after the sample measurement in the test sequence.[36] For isotopic measurements, the high-purity Mg solution Alfa-Mg was utilized as the bracketing standard. The $\delta^{26}Mg$ and $\delta^{25}Mg$ values of this solution were previously characterized at –1.40‰ ± 0.05‰ and –0.73‰ ± 0.03‰, respectively, against the DSM3 standard [30]. The conversion of the δ-value measured against Alfa-Mg to DSM3 follows the established relationship:

$$\delta^{x}\mathrm{Mg}_{\mathrm{DSM3}}(\mathrm{sample}) = \delta^{x}\mathrm{Mg}_{\mathrm{Alfa\text{-}Mg}}(\mathrm{sample}) + \delta^{x}\mathrm{Mg}_{\mathrm{DSM3}}(\mathrm{Alfa\text{-}Mg}) + \delta^{x}\mathrm{Mg}_{\mathrm{Alfa\text{-}Mg}}(\mathrm{sample}) \times \delta^{x}\mathrm{Mg}_{\mathrm{DSM3}}(\mathrm{Alfa\text{-}Mg}) \qquad (2)$$

Hereafter, the notations $\delta^{x}Mg_{DSM3}$ is abbreviated as $\delta^{x}Mg$. The reported $\delta^{x}Mg$ value for each sample represents the average of three times or more replicate measurements, and the analytical uncertainty is given as twice the standard deviation (2SD).

RESULTS AND DISCUSSION

Analytical accuracy and precision. The elution curve of Mg is presented in Fig.1. Through the purification, sequential elution of Na, Fe, K and Mg of sample was removed using the optimized acid mixture (Fig.1a). This method enables quantitative separation of Mg from others, which is essential for achieving accurate isotopic measurements and high recovery rates. To ensure data reliability, certified reference materials were incorporated throughout the analytical process for comprehensive quality control. Method validation included replicate analyses of the Alfa-Mg standard solution over a six-month period to monitor long-term analytical precision. The measurements shown a mean $\delta^{26}Mg$ value of –1.39‰ ± 0.06‰ (2SD, n = 113) (Fig. 1b), which aligns well with results from a previous study.[39]

Figure 2 displays the $\delta^{26}Mg$-$\delta^{25}Mg$ plot for all samples investigated in this study. The slope obtained from this plot falls within analytical uncertainty of the theoretically predicted mass fractionation coefficients for both kinetic (0.521) and equilibrium

Table 3. Mg isotopic comparison of reference materials in this study with published data

Sample	Description	Reference	δ^{26}Mg	2SD	δ^{25}Mg	2SD	n
BHVO-2	Basalt	This study	–0.23	0.03	–0.13	0.02	3
		Gao *et al.* [19]	–0.30	0.06	–0.14	0.05	3
		María *et al.* [56]	–0.20	0.03	–0.10	0.01	2
		An *et al.* [57]	–0.22	0.04	–0.10	0.03	14
		Pogge *et al.* [58]	–0.26	0.06	–0.14	0.04	4
BCR-2	Basalt	This study	–0.25	0.03	–0.14	0.03	3
		Gao *et al.* [19]	–0.23	0.06	–0.13	0.02	3
		Chapela *et al.* [56]	–0.29	0.08	–0.17	0.04	3
		Pogge *et al.* [58]	–0.25	0.04	–0.13	0.03	8
GSB-5	Cabbage	This study	–0.98	0.03	–0.51	0.03	3
		Liu *et al.* [30]	–1.00	0.03	–0.51	0.01	12
GSB-6	Spinach	This study	–0.84	0.05	–0.44	0.02	3
		Liu *et al.* [30]	–0.84	0.02	–0.43	0.01	12
GSB-14	Laver	This study	–0.83	0.03	–0.43	0.03	3
		Liu *et al.* [39]	–0.84	0.03	–0.44	0.01	12
GSB-11	Citrus leaf	This study	–1.04	0.04	–0.53	0.03	3
		Liu *et al.* [30]	–1.06	0.03	–0.55	0.03	12
GSB-19	Astragalus membranaceus	This study	–0.84	0.06	–0.43	0.04	4
		Liu *et al.* [39]	–0.79	0.04	–0.39	0.03	12
GSV-3	Bush leaves	This study	–1.05	0.06	–0.55	0.04	3
		Bao *et al.* [32]	–1.08	0.05	–0.54	0.06	3
Seawater		This study	–0.86	0.03	–0.45	0.03	3
		Gao *et al.* [19]	–0.83	0.12	–0.42	0.06	3
		Chapela *et al.* [56]	–0.85	0.02	–0.45	0.02	13
		Liu *et al.* [39]	–0.84	0.06	–0.44	0.03	36

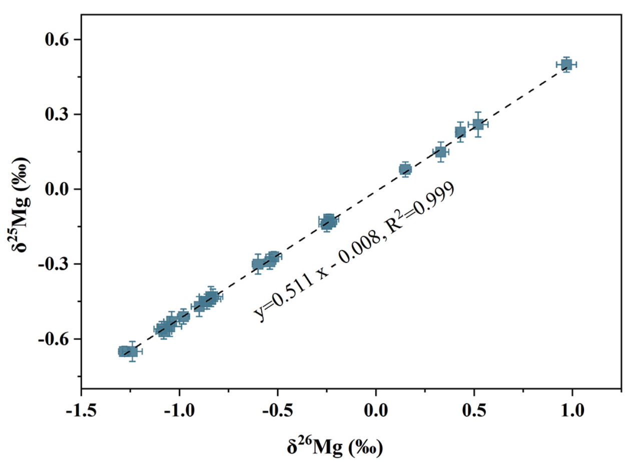

Fig. 2 Plot of δ^{26}Mg-δ^{25}Mg values for all samples analyzed in this study.

(0.510) fractionation.[40, 41] All analyzed reference materials showed fractionation behavior that followed the principles of mass dependence. These results confirm that the chromatographic separation method used in this study produces highly consistent and reproducible data, with high measurement accuracy and precision.

As shown in Table 3, δ^{26}Mg of a suite of biological and geological reference materials were precisely determined to further ensure the accuracy of the measurements. The measured reference materials including geochemical standards (basalts), a liquid standard (seawater), and biological standards (GSB-5, GSB-6, GSB-11, GSB-14, GSB-19, GSV-3). Our measurements yielded δ^{26}Mg values of –0.23‰ ± 0.03‰ for BHVO-2 and –0.25‰ ± 0.03‰ for BCR-2, with seawater displaying a value of –0.86‰ ± 0.03‰. The biological standards demonstrated characteristic isotopic compositions: GSB-5 (–0.98‰ ± 0.03‰), GSB-6 (–0.84‰ ± 0.05‰), GSB-11 (–1.04‰ ± 0.04‰), GSB-14 (–0.83‰ ± 0.03‰), GSB-19 (–0.84‰ ± 0.06‰), and GSV-3 (–1.05‰ ± 0.06‰). These results are in good agreement with published values [13, 19, 30, 32, 39], providing robust validation of the chemical purification and instrumental analysis methodologies employed in this study.

Mg isotopic compositions in reference materials. This study establishes an abundant Mg isotopic dataset for sixteen biological reference materials of critical importance to human diet and biogeochemical researches firstly. The newly characterized reference materials include rice flour (GSB-1, Element-ZK-004, BW2025-5051), scallop (GSB-15), shrimp (GSB-28), spirulina (GSB-16), milk powder (GSB-8), infant formula (BW2025-5050), chicken meat (GSB-9), pork liver (GSB-29), ginseng (GSB-18), tea leaves (GSV-4), bush branches and leaves (GSV-1) and human hairs (HHS-1, GBW09101). The Mg isotope compositions of these reference materials were shown in Table 4 and Fig. 3.

The δ^{26}Mg values reveal systematic variations between terrestrial and aquatic ecosystems with direct implications for human nutrition. Aquatic organisms, including laver (GSB-14, –0.83‰ ± 0.04‰), scallop (GSB-15, –1.09‰ ± 0.04‰), and shrimp (GSB-28, –1.08‰ ± 0.04‰), exhibit δ^{26}Mg values clustered around the seawater signature (–0.86‰ ± 0.03‰),

Table 4. Mg isotope ratio of biological reference materials

Sample	Description	n	δ²⁶Mg	2SD	δ²⁵Mg	2SD
GSB-1	Rice	3	0.33	0.04	0.15	0.04
Element-ZK-004	Rice Flour	3	0.52	0.05	0.26	0.04
BW2025-5051	Rice Flour	3	0.43	0.02	0.23	0.04
GSV-1	Bush Branches and Leaves	3	–1.28	0.03	–0.65	0.02
GSV-4	Tea Leaves	3	–0.52	0.04	–0.27	0.02
GBW10055	Full-fat Soybean Flour	3	0.15	0.03	0.08	0.03
GSB-8	Milk Powder	3	–0.60	0.03	–0.30	0.04
BW2025-5050	Infant Formula Powder	3	–0.54	0.03	–0.29	0.03
GSB-9	Chicken Meat	3	–0.24	0.05	–0.12	0.02
GSB-29	Pork Liver	3	0.97	0.05	0.50	0.03
GSB-15	Scallop	3	–1.09	0.04	–0.56	0.03
GSB-28	Prawn	3	–1.08	0.04	–0.57	0.03
GSB-16	Spirulina	3	–1.24	0.05	–0.65	0.04
GSB-18	Ginseng	3	–0.25	0.03	–0.14	0.03
HHS-1	Human Hair	3	–0.90	0.04	–0.47	0.04
GBW09101	Human Hair	3	–0.87	0.02	–0.45	0.02

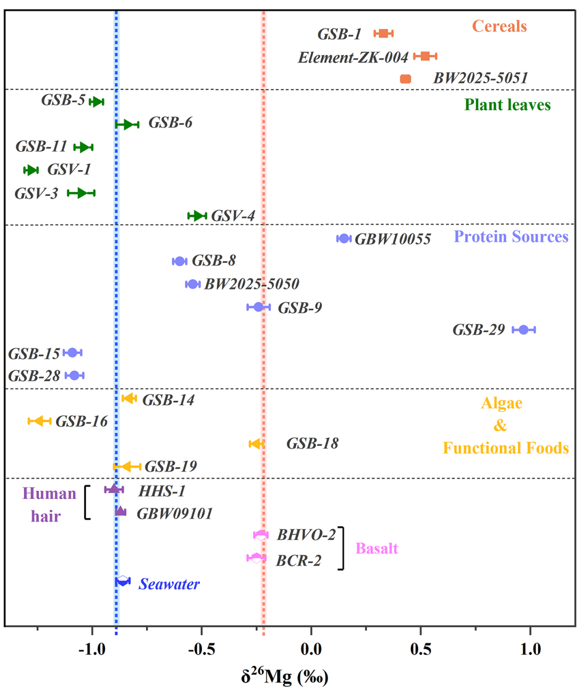

Fig. 3 The δ^{26}Mg values of reference materials determined in this study. The red and blue dashed line represent the mean δ^{26}Mg value of the bulk silicate Earth and seawater, respectively.

establishing a distinct isotopic end-member for aquatic-derived nutrients in human diets. Goff *et al.* [33] reported lighter values in fish products (–1.40‰ ± 0.25‰ ~ –0.87‰ ± 0.24‰), with the lightest signatures found in oyster hepatopancreas suggesting organ-specific fractionation. However, fish muscle proteins consistently approach seawater values, indicating minimal biological modification during intake. This consistency indicates that seawater composition exerts primary control on marine food sources, though variations exist among different marine organisms. Terrestrial plants display significant isotopic diversity exceeding 1.5‰ of δ^{26}Mg (Fig. 3), reflecting physiological processes relevant to nutritional quality.[42] Photosynthetic tissues (Spinach: –0.84‰ ± 0.05‰; Cabbage: –0.98‰ ± 0.03‰; Citrus leaf: –1.04‰ ± 0.04‰) are consistently enriched in light isotopes, demonstrating the characteristic fractionation associated with chlorophyll biosynthesis.[43] This pattern establishes plant leaves as the lighter Mg isotopic reservoir in human terrestrial diets. Conversely, rice-based staple foods (GSB-1, Element-ZK-004 and BW2025-5051, mean: –0.44‰ ± 0.16‰) show significantly heavier characteristic of storage organs with reduced fractionation. Our data further support that rice (–0.67‰ ± 0.05‰ [44]~ –0.33‰ ± 0.04‰) exhibits heavier isotopic values compared to wheat (–1.83‰ ~ –0.75‰),[19,26,30,45] which highlights Mg isotopic analyses as a useful tool for interpreting regional dietary Mg-intake patterns.

Animal products exhibit enrichment in heavier Mg isotopes along the trophic chain. Milk powder (GSB-8, –0.60‰ ± 0.03‰), infant formula (BW2025-5050, –0.54‰ ± 0.03‰), and chicken meat (GSB-9, –0.24‰ ± 0.05‰) show δ^{26}Mg values that are 0.3‰-0.8‰ heavier than their plant-based diets. This trend may reflect the preferential absorption of heavier isotopes during digestive processes that consistently observed in mammalian systems.[26] A particularly notable case is pork liver (GSB-29, 0.97‰ ± 0.05‰) exhibits a markedly enriched isotopic signature. This pattern is corroborated by findings in mouse models and minipig, where liver tissues consistently show the heaviest Mg isotopic signature within the body, amidst overall isotopic variations of approximately 1.5‰.[7, 21] The pronounced isotopic enrichment in liver tissues suggests significant organ-specific fractionation, potentially linked to specialized metabolic functions that could serve as indicators of metabolic health status.[46-48]

Human hair samples (HHS-1 and GBW09101, mean: –0.88‰ ± 0.04‰) present an integrated isotopic signature intermediate between major dietary end-members. This positioning likely represents the integration of lighter plant-derived isotopic signals with heavier animal-based Mg sources. Data from Japan, Belgium, and China indicate report hair reference values ranging from –0.81‰ ± 0.13‰ to –0.54‰ ± 0.11‰.[22] In addition, population datasets from Belgium and Sweden showing a broader range, from –1.03‰ to –0.15‰. Although human tissue data remain limited, hair isotopic compositions demonstrate considerable potential as biomarkers reflecting both dietary intake and metabolic processing.

These newly established Mg isotopic ratios provide a critical foundation for investigating nutritional metabolism and human health. The distinct isotopic signatures of major food groups enable tracking of Mg absorption from different dietary sources, while the systematic fractionation patterns between diet and biological tissues offer new avenues for developing isotopic biomarkers of metabolic function.

Application of Mg isotope in diet to human health. The analysis of biological samples including food crops, animal and human tissues, providing crucial insights into the global Mg cycle through their distinct Mg isotopic signatures. These biological materials exhibit significantly Mg isotopic fractionation, with the δ^{26}Mg values ranging from –1.28‰ to 0.97‰, a span of over 2.2‰ (Fig. 3), revealing a coherent narrative of isotopic fractionation across the biogeochemical cycle, from geological reservoirs to human biomarkers. This synthesis integrates these patterns to outline the dominant pathways and processes that shape Mg isotopic signatures, emphasizing their potential as tracers in nutritional and health studies.

The Mg isotopic cycle originates from geological reservoirs, characterized by relatively high δ^{26}Mg values (*e.g.*, mean of bulk silicate Earth: ~ –0.22‰).[42] Our data robustly confirm that photosynthetic tissues (*e.g.*, leaves) have low δ^{26}Mg values, with down to -1.28‰. In contrast, non-photosynthetic storage organs (*e.g.*, rice) exhibit heavier values. The Mg isotopic composition in plants is controlled by fractionation during key physiological processes, primarily root absorption and internal translocation.[49,50] During root absorption, Mg enters root cells predominantly via active transport through Mg-specific transporters (*e.g.*, MGT/MRS2 family proteins),[51] a process that favors the heavy isotope.[31] Following uptake, the transport of Mg from roots to aerial parts occurs as free hydrated Mg^{2+} via the transpiration stream in the xylem with limited isotope fractionation.[34] Consequently, aerial tissues (including grains, stems and leaves) generally exhibit lower δ^{26}Mg values than roots.[52] This pattern indicates the preferential translocation of light isotopes (^{24}Mg) within plant vascular systems.[34] In contrast, storage organs such as seeds and roots exhibit significantly heavier values due to weaker fractionation during deposition and storage, likely due to the formation of strong bonds between Mg^{2+} and organic ligands (*e.g.*, phytate in seeds, ATP/proteins in tissues) during deposition and storage, which thermodynamically favors the enrichment of ^{26}Mg.[27,31,34] This primary biological filtering establishes the foundational isotopic distribution of the human diet, where plant-based foods encompass a wide spectrum of δ^{26}Mg values, directly reflecting their physiological functions.

Trophic transfer of Mg through food chains alters its isotopic composition in animal tissues. Dairy products (–0.60 ± 0.03‰) and chicken meat (–0.24‰ ± 0.05‰) shows distinct δ^{26}Mg that differ from their plant-based diets. In animals, this shift may be attributed to preferential absorption of heavier isotopes (^{26}Mg) in the digestive system.[21,53] More pronounced isotopic fractionation occurs within animal bodies. An organ-specific fractionation is exemplified by the exceptionally heavy values in animal liver (0.27‰ ~ 0.97‰),[7,24] underscoring that internal metabolic processes can alter the isotopic composition. The enrichment of ^{26}Mg in the liver is thought to result from its sequestration into organelles and its preferential binding to enzymes and proteins involved in major metabolic pathways.[7] Conversely, muscle tissue, characterized by a large Mg pool with slow turnover, typically exhibits the lightest isotopic composition within the body.[21] As a central metabolic hub, the liver may preferentially retain or process ^{26}Mg through specific biochemical pathways, such as enzyme binding or sequestration into proteins.[8,46]

The human body integrates Mg from various biogeochemical pathways, with different tissues exhibiting characteristic Mg isotopic compositions that reflect their physiological roles. Hair reference materials measured in this study (δ^{26}Mg: –0.87‰ ± 0.02‰) along with reported dataset,[22] providing a stable record of long-term dietary intake due to their metabolic stability. This value lies within the reported range for diverse human tissues yet reveals distinct metabolic information. Blood (δ^{26}Mg: –0.26‰ ~ 0.06‰)[54] represent the circulating metabolic pool, showing heavier and less variable isotopic values. This characteristic likely reflects the immediate contribution of dietary end-members rich in heavy isotopes. In contrast, teeth[19] (–1.65‰ ~ –0.22‰) formed during childhood with minimal subsequent turnover, making δ^{26}Mg a more reliable indicator for revealing differences in individual early life. Kidney stones (–1.12‰ to –0.07‰) reveals strong localized fractionation under pathological conditions,[55] with preferential incorporation of lighter isotopes during crystallization. These tissue-specific patterns position Mg isotopes as a promising bridge between environmental geochemistry and human health, supporting source apportionment, metabolic fluxes quantification, and investigation of the isotopic manifestations of physiological disorders.

CONCLUSION

This study provides high-precision Mg isotope data for a diverse suite of biological and geological reference materials. The first-time measurements for major consumed foods and biological reference materials including rice flour, milk powder, infant formula, chicken, pork liver, scallop, shrimp, cabbage, ginseng, and human hair were reported. Our measurements show well agreement with available reference values, confirming the robustness of the analytical methodology. These results significantly expand the database of Mg isotopic compositions in biological standards, providing essential benchmarks for quality control and inter-laboratory comparisons in future Mg isotopic research. However, it should be noted that the current dataset primarily comprises commercially available reference materials with limited documentation of their geographical origins and ecological contexts. These findings underscore the capability of MC-ICP-MS to uncover biologically driven Mg isotope fractionation patterns across terrestrial and marine ecosystems. Overall, this work establishes a critical reference framework for applying Mg isotopes to investigate biogeochemical cycling, nutrient source apportionment, and metabolic studies across environmental and nutritional sciences.

AUTHOR INFORMATION

Guilin Han earned her Ph.D. from the Institute of Geochemistry, Chinese Academy of Sciences in 2003. She holds the title of "Outstanding Young Scientist" and "Changjiang Scholar" Professor at China University of Geosciences (Beijing). Her research focuses on the development and application of non-traditional isotope analytical techniques, using both traditional and non-traditional metal isotope geochemistry to investigate material cycling and interaction mechanisms between geological environments and human health. As the first or corresponding author, she has published more than 200 SCI-indexed papers, including two selected as ESI TOP 0.1% Hot Papers and 14 recognized as ESI TOP 1% Highly Cited Papers. Her pioneering work has greatly advanced isotope geochemistry and its application in environmental science and human health.

Corresponding Author

*G. L. Han

Email address: hanguilin@cugb.edu.cn

Notes

The authors declare no competing financial interest.

ACKNOWLEDGMENTS

We would like to modify the order of the fund support to: This work was supported by the China Postdoctoral Science Foundation (2025M770420), the "Deep-time Digital Earth" Science and Technology Leading Talents Team Funds for the Central Universities for the Frontiers Science Center for Deep-time Digital Earth, China University of Geosciences (Beijing) (2652023001), and the National Natural Science Foundation of China (4220301).

REFERENCES

1. M. S. Razzaque and S. J. Wimalawansa, *Nutrients*, 2025, **17**, 454. https://doi.org/10.3390/nu17030454
2. A. Deledda, E. Giordano, F. Velluzzi, G. Flore, S. Franceschelli, L. Speranza, and P. Ripari, *Int. J. Mol. Sci.*, 2022, **23**, 16219. https://doi.org/10.3390/ijms232416219
3. K. Nam, A. R. A. Thodika, S. Tischlik, C. Phoeurk, T. M. Nagy, L. Schierholz, J. Ådén, P. Rogne, M. Drescher, A. E. Sauer-Eriksson, and M. Wolf-Watz, *Sci. Adv.*, **10**, eado5504. https://doi.org/10.1126/sciadv.ado5504
4. B. R. Madhanagopal, H. Talbot, A. Rodriguez, J. M. Louis, H. Zeghal, S. Vangaveti, K. Reddy, and A. R. Chandrasekaran, *Nat. Commun.*, 2024, **15**, 6636. https://doi.org/10.1038/s41467-024-50348-3
5. S. L. Volpe, *Adv. Nutr.*, 2013, **4**, 378S-383S. https://doi.org/10.3945/an.112.003483
6. A. M. Al Alawi, S. W. Majoni, and H. Falhammar, *Int. J. Endocrinol.*, **2018**, 9041694. https://doi.org/10.1155/2018/9041694
7. S. le Goff, J.-P. Godin, E. Albalat, J. M. R. Nieves, and V. Balter, *Sci. Rep.*, 2022, **12**, 10941. https://doi.org/10.1038/s41598-022-14825-3
8. H. Geiger and C. Wanner, *Clin. Kidney J.*, 2012, **5**, 25-38. https://doi.org/10.1093/ndtplus/sfr165
9. J. H. F. de Baaij, J. G. J. Hoenderop, and R. J. M. Bindels, *Physiol. Rev.*, 2015, **95**, 1-46. https://doi.org/10.1152/physrev.00012.2014
10. G. Han and X. Li, *Sci. China Earth Sci.*, 2025, **55**, 4321-4333 https://doi.org/10.1071/s11430-025-1691-6
11. K. Weber, M. Weber, M. Menneken, A. G. Kral, R. Mertz-Kraus, T. Geisler, J. Vogl, and T. Tütken, *Chem. Geol.*, 2021, **572**. 120196. https://doi.org/10.1016/j.chemgeo.2021.120196
12. S. de Villiers, J. A. D. Dickson, and R. M. Ellam, *Chem. Geol.*, 2005, **216**, 133-142. https://doi.org/10.1016/j.chemgeo.2004.11.010
13. T. Gao, S. Ke, R. Li, X. n. Meng, Y. He, C. Liu, Y. Wang, Z. Li, and J.-M. Zhu, *Rapid Commun. Mass Spectrom.*, 2019, **33**, 767-777. https://doi.org/10.1002/rcm.8376
14. E. B. Bolou-Bi, N. Vigier, A. Poszwa, J.-P. Boudot, and E. Dambrine, *Geochim. Cosmochim. Acta*, 2012, **87**, 341-355. https://doi.org/10.1016/j.gca.2012.04.005
15. V. T. C. Chang, R. J. P. Williams, A. Makishima, N. S. Belshawl, and R. K. O'Nions, *Biochem. Biophys. Res. Commun.*, 2004, **323**, 79-85. https://doi.org/10.1016/j.bbrc.2004.08.053
16. K. E. Hansen, A. C. Nabak, R. E. Johnson, S. Marvdashti, N. S. Keuler, M. M. Shafer, and S. A. Abrams, *J. Nutr.*, 2014, **144**, 533-537. https://doi.org/10.3945/jn.113.186767
17. J. Feng, H. Wang, Z. Jing, Y. Wang, W. Wang, Y. Jiang, and W. Sun, *Front. Med.*, 2021, **8**, 626909. https://doi.org/10.3389/fmed.2021.626909
18. N. Yalçın, A. Ertınmaz Özkan, E. Güneş, and N. Koca, *Sci. Rep.*, 2025, **15**, 3545. https://doi.org/10.1038/s41598-025-86954-4

19. F. Gao, P. Zhang, K. Liu, X. Ling, and K.-J. Huang, *Front. Earth Sci.*, 2023, **10**, 1-11. https://doi.org/10.3389/feart.2022.1056881

20. K. V. Sullivan, R. E. T. Moore, and F. Vanhaecke, *Metallomics*, 2023, **15**, mfad012. https://doi.org/10.1093/mtomcs/mfad012

21. R. Grigoryan, M. Costas-Rodríguez, R. E. Vandenbroucke, and F. Vanhaecke, *Anal. Chim. Acta*, 2020, **1130**, 137-145. https://doi.org/10.1016/j.aca.2020.07.045

22. K. Rodiouchkina, I. Rodushkin, S. Goderis, and F. Vanhaecke, *Sci. Total Environ.*, 2022, **808**, 152059. https://doi.org/10.1016/j.scitotenv.2021.152059

23. R. Grigoryan, M. Costas-Rodríguez, S. Van Laecke, M. Speeckaert, B. Lapauw, and F. Vanhaecke, *J. Anal. At. Spectrom.*, 2019, **34**, 1514-1521. https://doi.org/10.1039/C9JA00097F

24. R. Grigoryan, M. Costas-Rodríguez, E. Van Wonterghem, R. E. Vandenbroucke, and F. Vanhaecke, *Front. Med.*, 2021, **8**, 664666. https://doi.org/10.3389/fmed.2021.664666

25. C. Weyh, K. Krüger, P. Peeling, and L. Castell, *Nutrients*, 2022, **14**, 644. https://doi.org/10.3390/nu14030644

26. J. E. Martin, D. Vance, and V. Balter, *Proc. Natl. Acad. Sci.*, 2015, **112**, 430-435. https://doi.org/10.1073/pnas.1417792112

27. J. R. Black, E. Epstein, W. D. Rains, Q.-z. Yin, and W. H. Casey, *Environ. Sci. Technol.*, 2008, **42**, 7831-7836. https://doi.org.10.1021/es8012722

28. R. Pokharel, R. Gerrits, J. A. Schuessler, P. J. Frings, R. Sobotka, A. A. Gorbushina, and F. von Blanckenburg, *Environ. Sci. Technol.*, 2018, **52**, 12216-12224. https://doi.org/10.1021/acs.est.8b02238

29. R. J. Tang and S. Luan, *Curr. Opin. Plant Biol.*, 2017, **39**, 97-105. https://doi.org/10.1016/j.pbi.2017.06.009

30. J. Liu and G. Han, *Geostand. Geoanal. Res.*, 2022, **46**, 535-545. https://doi.org/10.1111/ggr.12430

31. Y. Wang, B. Wu, A. E. Berns, Y. Xing, A. J. Kuhn, and W. Amelung, *Plant Soil*, 2020, **455**, 93-105. https://doi.org/10.1007/s11104-020-04604-2

32. Z. Bao, C. Zong, K. Chen, N. Lv, and H. Yuan, *Int. J. Mass Spectrom.*, 2020, **448**, 116268. https://doi.org/10.1016/j.ijms.2019.116268

33. S. Le Goff, E. Albalat, A. Dosseto, J.-P. Godin, and V. Balter, *Rapid Commun. Mass Spectrom.*, 2021, **35**, e9074. https://doi.org/10.1002/rcm.9074

34. Y. Fu, T. Gao, Q. Wu, M. Qi, Z. Wang, and C. Liu, *Sci. Total Environ.*, 2024, **923**, 171463. https://doi.org/10.1016/j.scitotenv.2024.171463

35. Y. An, X. Li, W. Lu, J. Xu, Y. Xue, Q. Gong, Y. Peng, F. Liu, M. Ling, and Z. Zhang, *Geostand. Geoanal. Res.*, 2024, **48**, 941-959. https://doi.org/10.1111/ggr.12582

36. F. Teng, W.-Y. Li, S. Ke, W. Yang, S. Liu, F. Sedaghatpour, S. Wang, K. Huang, Y. Hu, M. Ling, Y. Xiao, X. Liu, X. Li, H. Gu, C. K. Sio, D. A. Wallace, B. Su, L. Zhao, J. Chamberlin, M. Harrington, and A. Brewer, *Geostand. Geoanal. Res.*, 2015, **39**, 329-339. https://doi.org/10.1111/j.1751-908X.2014.00326.x

37. B. Guo, X. Zhu, A. Dong, B. Yan, G. Shi, and Z. Zhao, *J. Asian Earth Sci.*, 2019, **176**, 368-385. https://doi.org/10.1016/j.jseaes.2019.03.001

38. Q. Zhang, J. R. Liu, G. L. Han, T. Liang, and X. Q. Li, *Atom. Spectrosc.*, 2025, **46**, 258-266. https://doi.org/10.46770/as.2025.086

39. J. Liu and G. Han, *J. Anal. At. Spectrom.*, 2021, **36**, 1986-1995. https://doi.org/10.1039/d1ja00119a

40. M. Bizzarro, C. Paton, K. Larsen, M. Schiller, A. Trinquier, and D. Ulfbeck, *J. Anal. At. Spectrom.*, 2011, **26**, 565-577. https://doi.org/10.1039/C0JA00190B

41. F. Teng, *Rev. Mineral. Geochem.*, 2017, **82**, 219-287. https://doi.org/10.2138/rmg.2017.82.7

42. L. Chenzi, J. Zhangdong, G. Longfei, X. Yang, and Z. Fei, *Journal of Earth Environment*, 2024, **15**, 15-29. https://doi.org/10.7515/JEE221014

43. F. Moynier and T. Fujii, *Sci. Rep.*, 2017, **7**, 6973. https://doi.org/10.1038/s41598-017-07305-6

44. T. Gao, S. Ke, S.-J. Wang, F. Li, C. Liu, J. Lei, C. Liao, and F. Wu, *Geochim. Cosmochim. Acta*, 2018, **237**, 205-222. https://doi.org/10.1016/j.gca.2018.06.028

45. E. B. Bolou-Bi, N. Vigier, A. Brenot, and A. Poszwa, *Geostand. Geoanal. Res.*, 2009, **33**, 95-109. https://doi.org/10.1111/j.1751-908X.2009.00884.x

46. M. Liu, H. Yang, and Y. Mao, *Annal. Transl. Med.*, 2019, **7**, 578. https://doi.org/10.21037/atm.2019.09.70

47. S. C. Shah, X. Zhu, Q. Dai, R. M. Peek, and M. J. Shrubsole, *The Am. J. Clin. Nutr.*, 2021, **113**, 630-638. https://doi.org/10.1093/ajcn/nqaa326

48. N. S. Alzahrani, B. Aljahdali, A. Alhosain, A. A. Alasmari, T. Amna, and S. M. Yousef, *Pharmaceuticals*. 2025, **18**, 1196. https://doi.org/10.3390/ph18081196

49. S. Opfergelt, K. W. Burton, R. B. Georg, A. J. West, R. A. Guicharnaud, B. Sigfusson, C. Siebert, S. R. Gislason, and A. N. Halliday, *Geochim. Cosmochim. Acta*, 2014, **125**, 110-130. https://doi.org/10.1016/j.gca.2013.09.036

50. K. Wrobel, J. Karasiński, A. Tupys, M. A. Arroyo Negrete, L. Halicz, K. Wrobel, and E. Bulska, *Molecules*. 2020, **25**, 1644. https://doi.org/10.3390/molecules25071644

51. T. Saito, N. I. Kobayashi, K. Tanoi, N. Iwata, H. Suzuki, R. Iwata, and T. M. Nakanishi, *Plant Cell Physiol.*, 2013, **54**, 1673-1683. 10.1093/pcp/pct112

52. E. B. Bolou-Bi, A. Poszwa, C. Leyval, and N. Vigier, *Geochim. Cosmochim. Acta*, 2010, **74**, 2523-2537. https://doi.org/10.1016/j.gca.2010.02.010

53. J. E. Martin, D. Vance, and V. Balter, *Geochim. Cosmochim. Acta*, 2014, **130**, 12-20. https://doi.org/10.1016/j.gca.2013.12.029

54. N. Baharom and Y.-H. Yim, *Bull. Korean Chem. Soc.*, 2021, **42**, 1593-1601. https://doi.org/10.1002/bkcs.12410

55. J. Liu, G. Han, Y. Tian, R. Qu, D. Wang, and Y. Shen, *Metallomics*, 2024, **16**, mfae056. https://doi.org/10.1093/mtomcs/mfae056

56. M. Chapela Lara, H. L. Buss, P. A. E. Pogge von Strandmann, J. A. Schuessler, and O. W. Moore, *Geochim. Cosmochim. Acta*, 2017, **202**, 77-100. https://doi.org/10.1016/j.gca.2016.12.032

57. Y. An, F. Wu, Y. Xiang, X. Nan, X. Yu, J. Yang, H. Yu, L. Xie, and F. Huang, *Chem. Geol.*, 2014, **390**, 9-21. https://doi.org/10.1016/j.chemgeo.2014.09.014

58. P. A. E. Pogge von Strandmann, T. Elliott, H. R. Marschall, C. Coath, Y. Lai, A. B. Jeffcoate, and D. A. Ionov, *Geochim. Cosmochim. Acta*, 2011, **75**, 5247-5268. https://doi.org/10.1016/j.gca.2011.06.026